Impact of local thermal non-equilibrium on temporal thermo-hydro-mechanical processes in low permeable porous media

Xinle Zhai, and *Kamelia* Atefi-Monfared[*]

University at Buffalo, Department of Civil, Structural and Environmental Engineering, 14260 Buffalo NY, USA

Abstract. The thermo-hydraulic-mechanical (THM) response of low permeable media is of crucial significance in thermal fracturing for production of unconventional shale oil, enhanced geothermal systems, and waste disposal. During such processes, pore pressures and stresses change in a spatiotemporal manner due to hydraulic and thermal loadings. From the viewpoint of the energy balance equation, the available theoretical studies can be classified as local thermal equilibrium (LTE), and local thermal non-equilibrium (LTNE) models. LTE models consider identical temperature for different phase of the porous system. LTNE models allow different temperature variations in solid and fluid phases of a porous medium. Current LTNE studies are weakly-coupled – not incorporating thermo-osmosis. This paper presents novel coupled LTNE thermo-poroelastic solutions in a transversely isotropic saturated porous medium, incorporating thermo-osmosis effect. Solutions are obtained for permeable and impermeable boundaries. Thermo-osmosis is found to have a very different effect in case of LTNE versus LTE, resulting in a fundamentally different THM response. LTNE effect analysis reveals different THM responses under different heat transfer properties at the solid-fluid interface in low permeable strata.

1 Introduction

The thermo-hydraulic-mechanical (THM) behavior of low permeable media is of crucial significant in numerous projects including unconventional shale oil and tight sand [1], enhanced geothermal, and waste disposal [2, 3]. Numerous researchers have studied the THM response of the porous media under different conditions (loading, material anisotropy, wellbore inclination, and heat transfer mechanisms) using the thermo-poroelastic theory [4-9]. The majority of the relevant literature was developed assuming local thermal equilibrium (LTE), where identical temperature is assumed for both the solid and fluid phases. However, this assumption is contingent upon large interstitial heat transfer coefficients between different phases, and the porous formation to have higher ratios of pore surface area to pore volume.

Local Thermal Non-Equilibrium (LTNE) models are intended to elucidate the heat transfer between the solid phase and the fluid phase [10-14]. Due to the additional intricacy in the coupled response of the porous medium because of local thermal non-equilibrium, there are very few LTNE models developed, and are obtained based on a number of simplifying assumptions. No current LTNE model incorporates thermo-osmosis effects. Thermo-osmosis is a coupled process that is of significance in certain porous media, and is analogous to the Sorêt effect in solutions, which describes the influence of temperature gradient on fluid flow [15-21].

The current paper presents a new thermo-poroelastic theory to describe the THM response of transversely isotropic saturated porous media based on the LTNE theory, incorporating thermal osmosis. Analytical solutions are obtained using Laplace transform. The solutions are verified versus the results of Gao, et al. [1]. Finally, a comprehensive analysis is conducted to assess THM processes under LTE versus LTNE.

2 General formulations

2.1 Problem description

The problem of interest involves non-isothermal fluid injected into a saturated porous medium via a fully penetrating vertical wellbore. The porous formation is homogeneous, transversely isotropic, and linear elastic. Plane strain assumption is adopted. The permeability of formation is assumed $< 1 \times 10^{-18}$ m², making conduction the main heat transfer mechanism. Fluid and heat flow are assumed axisymmetric, and LTNE theory is adopted to consider the temperature difference between the solid phase and the pore fluid. Thermo-osmosis is considered in the formulations. The input parameters are those of Gao et al. [1, 21] and presented in Tab 1.

2.2 Constitutive equation

The constitutive relation describing the correlation between induced total stresses σ_{ij}, strains ε_{ij}, induced pore pressures P, and the solid phase induced temperature T_s for a transversely isotropic medium in a cylindrical coordinate system can be expressed as [22, 23]

---

[*] Corresponding author: kameliam@buffalo.edu

$$\begin{bmatrix} \sigma_{rr} \\ \sigma_{\theta\theta} \\ \sigma_{zz} \end{bmatrix} = \begin{bmatrix} M_{11} & M_{12} & M_{13} \\ M_{12} & M_{11} & M_{13} \\ M_{13} & M_{13} & M_{33} \end{bmatrix} \begin{bmatrix} \varepsilon_{rr} \\ \varepsilon_{\theta\theta} \\ \varepsilon_{zz} \end{bmatrix} - \begin{bmatrix} \alpha \\ \alpha \\ \alpha' \end{bmatrix} P - \begin{bmatrix} \beta^s \\ \beta^s \\ \beta^{s'} \end{bmatrix} T_s \quad (1)$$

where

$$\begin{cases} M_{11} = \dfrac{E\left(E'-Ev'^2\right)}{(1+\nu)\left(E'-E'\nu-2Ev'^2\right)} \\[2mm] M_{12} = \dfrac{E\left(E'\nu+Ev'^2\right)}{(1+\nu)\left(E'-E'\nu-2Ev'^2\right)} \\[2mm] M_{13} = \dfrac{EE'\nu'}{E'-E'\nu-2Ev'^2} \\[2mm] M_{33} = \dfrac{E'^2(1-\nu)}{E'-E'\nu-2Ev'^2} \end{cases} \quad (2)$$

$$\begin{cases} \alpha = 1 - \dfrac{M_{11}+M_{12}+M_{13}}{3K_s} \\[2mm] \alpha' = 1 - \dfrac{2M_{13}+M_{33}}{3K_s} \end{cases} \quad (3)$$

$$\begin{cases} \beta^s = \left(M_{11}+M_{12}\right)\alpha_{th}+M_{13}\alpha_{th}' \\[1mm] \beta^{s'} = 2M_{13}\alpha_{th}+M_{33}\alpha_{th}' \end{cases} \quad (4)$$

In Eqs. (1) - (4), M_{ij} is the drained elastic modulus coefficient; α and α' are Biot's effective stress coefficients in horizontal and vertical directions; β and β' are thermal coefficients of solid phase in horizontal and vertical directions; E and E' are the drained elastic modulus of rock in horizontal and vertical directions; ν and ν' are the Poisson's ratios of rock in horizontal and vertical directions; β^s and $\beta^{s'}$ represent thermal coefficients for the solid phase in horizontal and vertical directions; α_{th} and α_{th}' are linear expansion coefficients of the solid phase in horizontal and vertical directions. Note that tension is taken as positive sign convention.

Following the approach of Atefi Monfared and Rothenburg [24], we utilize the momentum equilibrium theorem, and the kinematic equations to obtain the following general differential equation

$$\frac{\partial^2 u_r}{\partial r^2} + \frac{1}{r}\frac{\partial u_r}{\partial r} - \frac{u_r}{r^2} = \frac{1}{M_{11}}\left(\alpha\frac{\partial P}{\partial r}+\beta^s\frac{\partial T_s}{\partial r}\right) \quad (5)$$

Integrating Eq. (5) over radius results in the following differential equation for the radial displacement

$$\frac{\partial u_r}{\partial r} + \frac{u_r}{r} = Y_1 P + Y_2 T_s \quad (6)$$

where

$$\begin{cases} Y_1 = \dfrac{\alpha}{M_{11}} \\[2mm] Y_2 = \dfrac{\beta^s}{M_{11}} \end{cases} \quad (7)$$

2.3 Fluid diffusion equation

In the LTNE theory, pore pressures are related to the fluid content, rock deformation, rock temperature, and the pore fluid temperature as demonstrated in Eq. (8) [1]

$$P = M\left[\zeta - \alpha\left(\varepsilon_{rr}+\varepsilon_{\theta\theta}\right)+\alpha_\phi T_s+\phi_0\alpha^f T_f\right] \quad (8)$$

Table 1. Reservoir information and rock properties [1, 31].

Fluid and Rock properties	
Porosity, φ_o	0.1
Elastic modulus of rock, E	20.6 GPa
Poisson's ratio of rock, ν	0.19
Linear thermal expansion coefficient of rock, α_{th}	6×10^{-6} /K
Volumetric thermal expansion coefficient of fluid, α^f	3.1×10^{-4} /K
Permeability, k	1×10^{-5} mD
Fluid viscosity, μ	1×10^{-3} Pa·s
Non-dimensional solid-fluid transfer coefficient, $h*$	1.0
Thermo-osmosis coefficient, K_{PT}	1.6×10^{-11} m²/(K·s)
Thermal conductivity of solid and fluid, λ_s, λ_f	1.3, 0.58 W/(m·K)
Solid and fluid densities, ρ_s, ρ_f	2710, 1113 kg/m³
Specific heat of rock and fluid, C_s, C_f	768, 4180 J/(kg·K)
Bulk modulus of grain and fluid, K_s, K_f	48.21, 2.15 GPa
Modulus ratio, E/E'	1.0
Ratio of Poisson's ratio, ν/ν'	1.0
Thermal expansion ratio, α_{th}/α_{th}'	1.0
Geometry, Initial state, Source parameters	
Wellbore radius, a	0.1 m
Initial pore pressure, P_0	24 MPa
Initial temperature of formation, T_0	85 ºC
Wellbore pressure (Source), P_w	29 MPa
Wellbore temperature (Source), T_w	125 ºC

where

$$M = \frac{K_s}{\left(1-M_{iijj}/9K_s\right)-\phi_0\left(1-K_s/K_f\right)} \quad (9)$$

$$\alpha_\phi = 2\left(\alpha-\phi_0\right)\alpha_{th}+\left(\alpha'-\phi_0\right)\alpha_{th}' \quad (10)$$

$$M_{iijj} = 2M_{11}+2M_{12}+4M_{13}+M_{33} \quad (11)$$

M is Biot's modulus; T_f is pore fluid temperature; K_f is the bulk modulus of the pore fluid; α_ϕ is the thermic coefficient of the pore space; and ζ is the variation of the pore fluid content. The rate of change of fluid content is accompanied by divergence of fluid flux

$$\frac{\partial \zeta}{\partial t}+\nabla\cdot\mathbf{q^f}=0 \quad (12)$$

where $\nabla\cdot$ is the divergence vector operator, and $\nabla\cdot=\partial/\partial r$ for axisymmetric flow; and $\mathbf{q^f}$ is the total pore fluid flux vector. If we incorporate thermo-osmosis, $\mathbf{q^f}$ becomes a function of pore pressure gradients and pore fluid temperature gradients as follows [15]

$$\mathbf{q^f} = -\frac{k}{\mu}\nabla P - K_{PT}\nabla T_f \quad (13)$$

where ∇ is the gradient vector operator. K_{PT} is referred to as the thermo-osmosis coefficient, and is related to enthalpy and the permeability coefficient. K_{PT} may be

positive or negative [18], with an absolute reported value ranging from 1×10^{-14} to 1×10^{-10} m²/(K·s) [25].

Combining Eqs. (8), (12) and (13), results in the following equation relating the induced pore pressures, strains, and temperatures of the solid and fluid phases

$$\frac{k}{\mu}\nabla^2 P + K_{PT}\nabla^2 T_f = \frac{1}{M}\frac{\partial P}{\partial t} - \alpha_\phi \frac{\partial T_s}{\partial t} - \phi_0 \alpha^f \frac{\partial T_f}{\partial t} \\ + \alpha \frac{\partial(\varepsilon_{rr} + \varepsilon_{\theta\theta})}{\partial t} \quad (14)$$

where $\nabla^2 = \nabla \cdot \nabla = \frac{\partial^2}{\partial r^2} + \frac{1}{r}\frac{\partial}{\partial r}$ is the Laplace operator.

Combining Eqs. (6) and (14), we obtain the fluid diffusion equation

$$\nabla^2 P + \frac{\mu}{k}K_{PT}\nabla^2 T_f = \frac{\mu}{k}\left(\frac{1}{M} + \alpha Y_1\right)\frac{\partial P}{\partial t} \\ - \frac{\mu}{k}\left(\alpha_\phi - \alpha Y_2\right)\frac{\partial T_s}{\partial t} - \frac{\mu}{k}\phi_0 \alpha^f \frac{\partial T_f}{\partial t} \quad (15)$$

2.4 Heat diffusion equation

The total heat flux of the solid phase $\mathbf{q_s^h}$ can be described based on the thermal conductivity of solid phase λ_s as

$$\mathbf{q_s^h} = -(1-\phi_0)\lambda_s \nabla T_s \quad (16)$$

Specific entropy of rock e_s^d is related to rock temperature, rock deformation, and pore pressure through [26, 27]:

$$e_s^d = \frac{(1-\phi_0)\rho_s^0 C_s}{T_s^0}T_s - \alpha_\phi P \quad (17)$$

where e_s^d is the specific entropy of rock; ρ_s^0 is the initial rock density; C_s is the specific heat of rock, and T_s^0 is the initial rock temperature. Here we neglect the effect of rock deformation on e_s^d (heat sink effect).

The heat energy conversation of solid phase based on the LTNE theory is described as

$$T_s^0 \frac{\partial e_s^d}{\partial t} + \nabla \cdot \mathbf{q_s^h} + h_{int}\left(T_s - T_f\right) = 0 \quad (18)$$

The parameter h_{int} is the heat transfer coefficient related to the solid-fluid interface, and expressed as [1]

$$h_{int} = \frac{\phi_0 \rho_f^0 C_f h^* c_h}{a^2} \quad (19)$$

where a is the wellbore radius; h^* is the non-dimensional solid-fluid transfer coefficient and assumed to be 1 in this paper following Gao, et al. [1]. Later in this paper, we assess the sensitivity of the THM response based on the h^* parameter. c_h is the thermal diffusivity of the rock mass and computed using the proposed equation by Carson, et al. [28]. Gao et al. [1] obtained Eq. (19) by performing the non-dimensional operation on Eq. (20) and Eq. (24), where it was revealed that the h_{int} parameter is impacted by the wellbore radius.

Combining Eqs. (16), (17) and (18), the heat diffusion equation for the solid phase is

$$\nabla^2 T_s = \frac{\rho_s^0 C_s}{\lambda_s}\frac{\partial T_s}{\partial t} - \frac{\alpha_\phi T_s^0}{(1-\phi_0)\lambda_s}\frac{\partial P}{\partial t} + \frac{h_{int}}{(1-\phi_0)\lambda_s}\left(T_s - T_f\right) \quad (20)$$

The total heat flux of the fluid phase can be expressed as

$$\mathbf{q_f^h} = -\phi_0 \lambda_f \nabla T_f \quad (21)$$

where $\mathbf{q_f^h}$ is the total heat flux vector of pore fluid.

The specific entropy of the fluid phase is related to the fluid temperature and pore pressure as

$$e_f^d = \frac{\phi_0 \rho_f^0 C_f}{T_f^0}T_f - \phi_0 \alpha^f P \quad (22)$$

In case of LTNE, the heat energy conversation of the fluid phase can be described as

$$T_f^0 \frac{\partial e_f^d}{\partial t} + \nabla \cdot \mathbf{q_f^h} + h_{int}\left(T_f - T_s\right) = 0 \quad (23)$$

Combining Eqs. (21), (22) and (23) and after some manipulations, we are able to obtain the heat diffusion equation for the pore fluid as

$$\nabla^2 T_f = \frac{\rho_f^0 C_f}{\lambda_f}\frac{\partial T_f}{\partial t} - \frac{T_f^0 \alpha^f}{\lambda_f}\frac{\partial P}{\partial t} + \frac{h_{int}}{\phi_0 \lambda_f}\left(T_f - T_s\right) \quad (24)$$

2.5 General solution

Thus far, we derived general equations for fluid diffusion Eq. (15); heat diffusion of the solid phase Eq. (20); and heat diffusion of the pore fluid Eq. (24). These general equations can be presented using the matrix form as

$$\begin{bmatrix} 1 & 0 & \frac{\mu}{k}K_{PT} \\ 0 & 1 & 0 \\ 0 & 0 & 1 \end{bmatrix}\nabla^2\begin{pmatrix} P \\ T_s \\ T_f \end{pmatrix} = \begin{bmatrix} c_1 & -c_2 & -c_3 \\ c_4 & c_5 & 0 \\ -c_6 & 0 & c_7 \end{bmatrix}\frac{\partial}{\partial t}\begin{pmatrix} P \\ T_s \\ T_f \end{pmatrix} \quad (25)$$

$$+\begin{bmatrix} 0 & 0 & 0 \\ 0 & c_8 & -c_8 \\ 0 & -c_9 & c_9 \end{bmatrix}\begin{pmatrix} P \\ T_s \\ T_f \end{pmatrix}$$

where

$$\begin{cases} c_1 = \frac{\mu}{k}\left(\frac{1}{M} + \alpha Y_1\right) \\ c_2 = \frac{\mu}{k}\left(\alpha_\phi - \alpha Y_2\right) \\ c_3 = \frac{\mu}{k}\phi_0 \alpha^f \end{cases} \quad (26)$$

$$\begin{cases} c_4 = -\frac{\alpha_\phi T_s^0}{(1-\phi_0)\lambda_s} \\ c_5 = \frac{\rho_s^0 C_s}{\lambda_s} \end{cases} \quad (27)$$

$$\begin{cases} c_6 = \frac{T_f^0 \alpha^f}{\lambda_f} \\ c_7 = \frac{\rho_f^0 C_f}{\lambda_f} \end{cases} \quad (28)$$

$$\begin{cases} c_8 = \frac{h_{int}}{(1-\phi_0)\lambda_s} \\ c_9 = \frac{h_{int}}{\phi_0 \lambda_f} \end{cases} \quad (29)$$

Applying Laplace transform to Eq. (25) results in

$$\nabla^2 \mathbf{\Psi} = \mathbf{\Lambda}\mathbf{\Psi} \quad (30)$$

where s is Laplace transform parameter and

$$\mathbf{\Psi} = \begin{pmatrix} \bar{P} & \bar{T_s} & \bar{T_f} \end{pmatrix}^T \quad (31)$$

$$\mathbf{\Lambda} = \begin{bmatrix} 1 & 0 & -\frac{\mu}{k}K_{PT} \\ 0 & 1 & 0 \\ 0 & 0 & 1 \end{bmatrix}\begin{bmatrix} c_1 s & -c_2 s & -c_3 s \\ c_4 s & c_5 s + c_8 & -c_8 \\ -c_6 s & -c_9 & c_7 s + c_9 \end{bmatrix} \quad (32)$$

It should be noted that we assume the initial state of the reservoir to be homogeneous. Pore pressures, and

temperatures in Eq. (25) are induced values, thus the initial term due to Laplace transform will be zero. We can find from Eq. (32) that matrix $\mathbf{\Lambda}$ is independent of time and space. We assume $\mathbf{\Psi}$ can be expressed in terms of the modified Bessel function of the second kind in the following manner

$$\mathbf{\Psi} = \mathbf{X} K_0\left(r\sqrt{q}\right) \tag{33}$$

where $\mathbf{X}$ is a column vector with three rows, and $K_0\left(x\right)$ is the modified Bessel function of the second kind (zero-order). Substituting Eq. (33) into Eq. (30) results in

$$\nabla^2 \mathbf{\Psi} = q\mathbf{X} K_0\left(r\sqrt{q}\right) = \mathbf{\Lambda} \mathbf{X} K_0\left(r\sqrt{q}\right) \tag{34}$$

Dividing Eq. (34) by the non-zero term $K_0\left(r\sqrt{q}\right)$, the relation between $\mathbf{\Lambda}$ and q is obtained as follows

$$\mathbf{\Lambda} \mathbf{X} = q\mathbf{X} \tag{35}$$

For the purpose of the current study, we chase for a nontrivial solution where $\mathbf{X} \neq 0$. Hence, we need to obtain the eigenvalues and eigenvectors of matrix $\mathbf{\Lambda}$. Assuming $\mathbf{\Lambda}$ is a non-singular matrix, it has three eigenvalues q_i with corresponding eigenvectors $\mathbf{X}_i$ (i=1, 2, 3). We define matrix $\mathbf{Q}$ to be composed of the eigenvectors $\mathbf{X}_i$. Therefore, the solution of Eq. (30) can thus be expressed as

$$\mathbf{\Psi} = \mathbf{Q} \begin{bmatrix} K_0\left(r\sqrt{q_1}\right) & & \\ & K_0\left(r\sqrt{q_2}\right) & \\ & & K_0\left(r\sqrt{q_3}\right) \end{bmatrix} \begin{pmatrix} A_1 \\ A_2 \\ A_3 \end{pmatrix} \tag{36}$$

where the parameter vector $\left(A_1 \quad A_2 \quad A_3\right)^T$ are constants and related to boundary conditions, and are independent of space and time in this study. Specific solutions to Eq. (36) can be obtained based on fluid and heat boundary conditions, as explained next.

2.5.1 Permeable boundary condition (PBC)

The PBC implies constant pore pressure and temperature at the wellbore, as expressed in Eq. (37)

$$\begin{cases} P\big|_{r=a} = P_w - P_0 \\ T_s\big|_{r=a} = T_f\big|_{r=a} = T_w - T_0 \\ T_s^0 = T_f^0 = T_0 \end{cases} \tag{37}$$

where T_0 is the initial in-situ temperature of the formation prior to implementation of the heat source. Combining Eqs. (36) and (37), we obtain that

$$\begin{pmatrix} P \\ T_s \\ T_f \end{pmatrix} = L^{-1}$$

$$\left\{ \frac{1}{s} \mathbf{Q} \begin{bmatrix} \frac{K_0\left(r\sqrt{q_1}\right)}{K_0\left(a\sqrt{q_1}\right)} & & \\ & \frac{K_0\left(r\sqrt{q_2}\right)}{K_0\left(a\sqrt{q_2}\right)} & \\ & & \frac{K_0\left(r\sqrt{q_3}\right)}{K_0\left(a\sqrt{q_3}\right)} \end{bmatrix} \mathbf{Q}^{-1} \begin{pmatrix} P_w - P_0 \\ T_w - T_0 \\ T_w - T_0 \end{pmatrix} \right\} \tag{38}$$

where L^{-1} is the inverse Laplace transform.

2.5.2 Impermeable boundary condition (IMPBC)

Under this boundary condition, the pore pressure, rock temperature, and fluid temperature at the wellbore satisfy the following criteria

$$\begin{cases} \dfrac{\partial P}{\partial r}\bigg|_{r=a} = 0 \\ T_s\big|_{r=a} = T_f\big|_{r=a} = T_w - T_0 \\ T_s^0 = T_f^0 = T_0 \end{cases} \tag{39}$$

By combining Eqs. (36) and (39) and applying inverse Laplace transform, P, T_s, and T_f under IMPBC are therefore obtained as

$$\begin{pmatrix} P \\ T_s \\ T_f \end{pmatrix} = L^{-1}$$

$$\left\{ \frac{1}{s} \mathbf{Q} \begin{bmatrix} -Q(1,1)\frac{\sqrt{q_1}K_1\left(a\sqrt{q_1}\right)}{K_0\left(r\sqrt{q_1}\right)} & -Q(1,2)\frac{\sqrt{q_2}K_1\left(a\sqrt{q_2}\right)}{K_0\left(r\sqrt{q_2}\right)} & -Q(1,3)\frac{\sqrt{q_3}K_1\left(a\sqrt{q_3}\right)}{K_0\left(r\sqrt{q_3}\right)} \\ Q(2,1)\frac{K_0\left(a\sqrt{q_1}\right)}{K_0\left(r\sqrt{q_1}\right)} & Q(2,2)\frac{K_0\left(a\sqrt{q_2}\right)}{K_0\left(r\sqrt{q_2}\right)} & Q(2,3)\frac{K_0\left(a\sqrt{q_3}\right)}{K_0\left(r\sqrt{q_3}\right)} \\ Q(3,1)\frac{K_0\left(a\sqrt{q_1}\right)}{K_0\left(r\sqrt{q_1}\right)} & Q(3,2)\frac{K_0\left(a\sqrt{q_2}\right)}{K_0\left(r\sqrt{q_2}\right)} & Q(3,3)\frac{K_0\left(a\sqrt{q_3}\right)}{K_0\left(r\sqrt{q_3}\right)} \end{bmatrix}^{-1} \begin{pmatrix} 0 \\ T_w - T_0 \\ T_w - T_0 \end{pmatrix} \right\} \tag{40}$$

We adopt the approximate formulae proposed by Valsa and Brančik [29] to compute numerically the inverse Laplace transform. It should be noted that the $h*$ value, which governs heat transfer between the solid and fluid phases, controls the status of LTNE. A very high $h*$ value replicates LTE [9]. The LTE status for THM analysis in this paper is obtained as such.

3 Results and Discussion

3.1 Model verification

There is currently no LTNE model that incorporates thermo-osmosis. For model verification, we have adopted the results presented by Gao, et al. [1]. We choose the thermo-osmosis coefficient to be zero in our model, and adopt the special case solutions of Eq. (38) for this verification. Input parameters are presented in Tab 1.
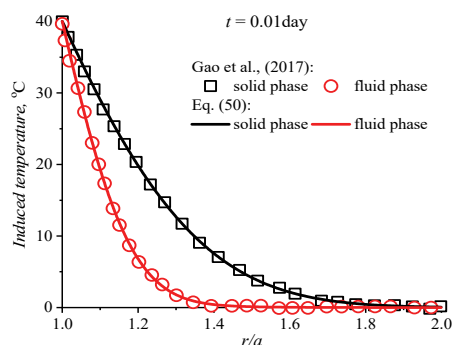

Fig 1. Verification of the proposed fluid and solid temperature equations against Gao, et al. [1].

Fig. 1 presents temperature distributions of the solid matrix as well as that of the in-situ fluid phase at time 0.01 day. Results demonstrate a good accordance between our proposed solutions and the values by Gao et al. [1].

3.2 LTNE results versus LTE results

To demonstrate the impact of LTNE on formation's response, temperatures, pore pressures, and stresses are computed under LTNE ($h^* = 1$) and compared against those of LTE ($h^* = 1000$). Thermo-osmosis has been incorporated for this assessment. Fig 2 illustrates temperature distributions for both PBC and IMPBC.
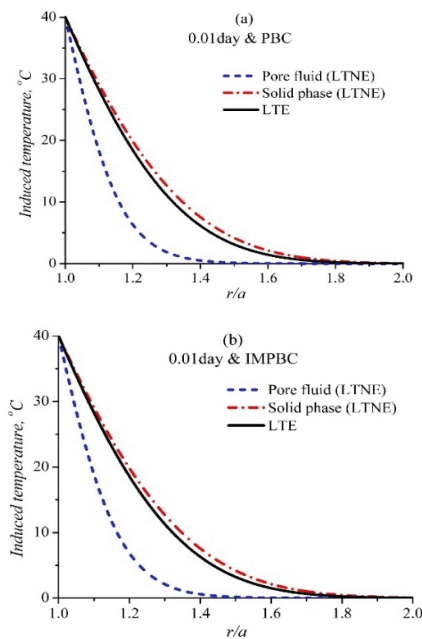
Fig 2. Temperature distributions based on LTNE versus LTE theories.

At early times subsequent to implementation of heat source – independent of the fluid boundary – the temperature of the pore fluid is notably lower compared to that of the solid phase under LTNE. This is due to higher thermal conductivity of the solid phase compared to the fluid, leading to a more rapid heat transmission. LTE results in in-situ temperatures that are slightly lower compared to those of the solid phase from LTNE, but significantly higher than those of the fluid phase. The temperature of the solid phase is much closer to the results from LTE compared to the fluid temperatures.

Next, we assess the significance of the thermo-osmosis under LTNE. To achieve this, the corresponding values from LTE have been subtracted from the presented results. Fig. 3 illustrates induced pore pressures and effective stresses under both PBC and IMPBC boundary conditions for two case scenarios: conventional thermo-poroelasticity (trivial thermal osmosis); and incorporating thermal osmosis. This analysis is conducted for 0.01 day and 0.1 day. Fig. 3a reveals that even under conventional thermo-poroelasticity (trivial thermo-osmosis), LTNE influences pore pressure and stress variations (maximum

3 MPa at 0.01 day). This observation is consistent with previous studies [30]. Lower pore pressures are generated under LTNE compared to LTE when ignoring the non-traditional thermal process. This is due to the notably smaller temperature gradients in the former as a result of the gradual heat exchange between the two phases.

Fig. 3b reveals a much higher impact (maximum 20 MPa difference between induced stresses at 0.01 day) from thermo-osmosis. This thermal mechanism results in notably higher pore pressures under LTNE versus LTE. For later times (0.1 day), the results (Fig. 3c) reveal a substantial difference between the induced geomechanical alterations under LTNE versus LTE. Incorporating thermo-osmosis results in notably higher pore pressure generation under LTNE versus LTE. This difference is much more significant under IMPBC, and could be as high at 20 MPa in the induced tangential stress at source vicinity for the adopted input parameters. Findings suggest that thermo-osmosis results in a fundamentally different THM response under LTNE.
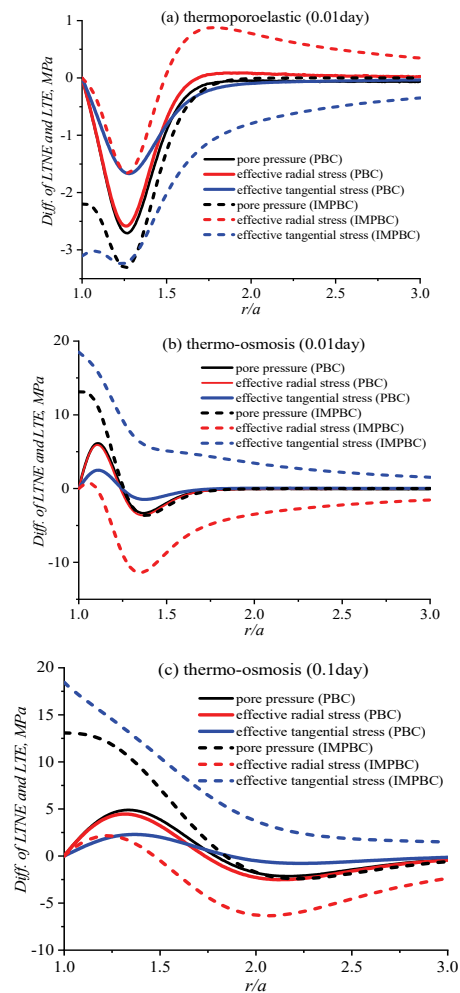

Fig 3. Induced pore pressure and stresses under various thermal related processes.

4 LTNE effect sensitivity

Next, we assess the impact of $h*$ on the THM response of porous medium. Fig. 4 shows notably higher pore pressures induced under a smaller $h*$ value compared to LTE results. This is due to higher solid temperatures and thermo-osmosis effect. LTNE results yield to those of LTE with $h*$ value increasing. A higher $h*$ value is required under IMPBC for the formation to reach LTE compared to PBC.
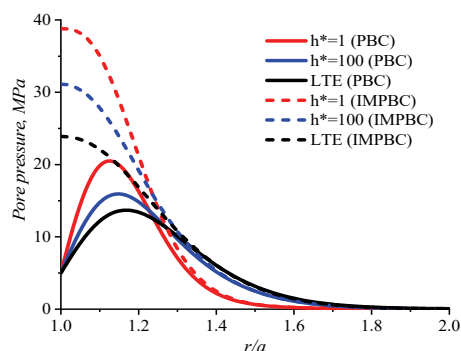

Fig 4. Induced pore pressure distributions with different $h*$ values (t=0.01 day).

5 Conclusions

This paper presents new fully-coupled thermo-poroelastic solutions under LTNE, incorporating thermo-osmosis for the first time. Formulations are obtained for a transversely isotropic saturated porous medium, subjected to a vertical heat and fluid line source. Specific solutions are obtained for permeable and impermeable hydraulic boundary conditions. The following are key observations:

- Under LTNE, a saturated porous formation subjected to heat source undergoes notably lower pore fluid temperatures compared to LTE, while the solid temperatures are slightly higher from the former.
- Thermo-osmosis results in generation of notably higher pore pressures under LTNE versus LTE, whereas ignoring thermo-osmosis causes lower pore pressures induced under LTNE compared to LTE.
- A higher solid-fluid transfer coefficient $h*$ increases fluid temperature substantially, while slightly decreasing solid temperature. Notably higher pore pressures and stresses are induced under a smaller $h*$ value ($h*=1$).

References

1. J. Gao, J. Deng, K. Lan, Y. Feng, W. Zhang and H. Wang, *Int. J. Rock Mech. Min. Sci.*, **96**, 66-84 (2017).
2. B. François, L. Laloui and C. Laurent, *Comput. Geotech.*, **36**, 626-640 (2009).
3. A. P. Selvadurai and A. Suvorov, *Thermo-poroelasticity and geomechanics*, Cambridge University Press, 2017.
4. Y. Abousleiman, S. K. Hoang and C. Liu, *Int. J. Numer. Anal. Methods Geomech.*, **38**, 493-517 (2014).
5. M. F. Ghasemi, M. M. Ghiasi, A. H. Mohammadi, A. Garavand and Y. Noorollahi, *J. Nat. Gas Sci. Eng.*, **52**, 559-574 (2018).
6. J. R. Rice and M. P. Cleary, *Rev. Geophys.*, **14**, 227-241 (1976).
7. X. Zhai and K. Atefi-Monfared, *Int. J. Rock Mech. Min. Sci.*, **126**, 104173 (2020).
8. X. Zhai and K. Atefi-Monfared, *Int. J. Heat Mass Transf.*, **150**, 119278 (2020).
9. X. Zhai and K. Atefi-Monfared, *Comput. Geotech.*, **122**, 103501 (2020).
10. P.-X. Jiang and Z.-P. Ren, *Int. J. Heat Fluid Flow*, **22**, 102-110 (2001).
11. B. Alazmi and K. Vafai, *Int. J. Heat Mass Transf.*, **45**, 3071-3087 (2002).
12. L.-W. He and Z.-H. Jin, *Int. J. Eng. Sci.*, **49**, 240-252 (2011).
13. Z.-H. Jin and L.-W. He, *Acta Mech.*, **224**, 1429-1439 (2013).
14. A. Gandomkar and K. Gray, *Geomech. Energy Envir.*, **20**, 100135 (2019).
15. Y. Zhou, R. Rajapakse and J. Graham, *Int. J. Solids Struct.*, **35**, 4659-4683 (1998).
16. C. Dirksen, *SPE. J.*, **33**, 821-826 (1969).
17. J. Trémosa, J. Gonçalvès, J. Matray and S. Violette, *J. Colloid Interface Sci.*, **342**, 175-184 (2010).
18. J. Gonçalvès and J. Trémosa, *J. Colloid Interface Sci.*, **342**, 166-174 (2010).
19. J. Gonçalvès, G. de Marsily and J. Tremosa, *Earth Planet Sci. Lett.*, **339**, 1-10 (2012).
20. Y. Yang, K. Guerlebeck and T. Schanz, *Transp. Porous Media*, **104**, 253-271 (2014).
21. J. Gao, J. Deng, K. Lan, Z. Song, Y. Feng and L. Chang, *Geothermics*, **67**, 114-134 (2017).
22. O. Coussy, *Transp. Porous Media*, **4**, 281-293 (1989).
23. O. Coussy and F. Ulm, *Mechanics of porous continua*, Wiley Chichester, 1995.
24. K. Atefi Monfared and L. Rothenburg, *SPE J.*, **22**, 184-197 (2017).
25. J. M. Soler, *J. Contam. Hydrol.*, **53**, 63-84 (2001).
26. Z. Song, F. Liang and S. Chen, *Comput. Geotech.*, **112**, 93-103 (2019).
27. M. A. Biot, *J. Appl. Phys.*, **27**, 240-253 (1956).
28. J. K. Carson, S. J. Lovatt, D. J. Tanner and A. C. Cleland, *Int. J. Heat Mass Transf.*, **48**, 2150-2158 (2005).
29. J. Valsa and L. Brančik, *Int. J. Numer. Model. El.*, **11**, 153-166 (1998).
30. A. Gandomkar and K. Gray, *Int. J. Heat Mass Transf.*, **124**, 1212-1216 (2018).